LAWRENCE
LIVERMORE
NATIONAL
LABORATORY

LLNL-CONF-490513

Next Generation Waveform Based Three-Dimensional Models and Metrics to Improve Nuclear Explosion Monitoring in the Middle East

B. Savage, D. Peter, B. Covellone, A. J. Rodgers, J. Tromp

July 11, 2011

Monitoring Research Review
Tucson, AZ, United States
September 13, 2011 through September 15, 2011

Disclaimer

NEXT GENERATION WAVEFORM BASED THREE-DIMENSIONAL MODELS AND METRICS TO IMPROVE NUCLEAR EXPLOSION MONITORING IN THE MIDDLE EAST

Brian Savage[1], Daniel Peter[2], Brian Covellone[1] Arthur Rodgers[3], and Jeroen Tromp[2]

University of Rhode Island[1], Princeton University[2], and Lawrence Livermore National Laboratory[3]

Sponsored by the Air Force Research Laboratory

Sponsored by the National Nuclear Security Administration

Contract No. FA8718-08-C-0009.

ABSTRACT

Improving the current Middle East wave speed with full waveforms required confidence in sources and recordings, along with a methodology to iteratively improve the model and reducing its minimum period. Recordings of seismic waves traversing the region from Tibet to the Red Sea and their mismatch compare to synthetics from the current iteration model are the principal metric in improving the current wave speed model. To avoid a mapping of source errors into the new wave speed model, a rigorous characterization of each source within the current wave speed model was undertaken. Source depths and paths near nodal planes are error prone as small changes may affect the resulting wavefield. After the sources were evaluated, regions requiring refinement were highlighted using adjoint tomography methods based on spectral element simulations [Komatitsch and Tromp (1999)].

We reinterpreted a large, well recorded subset of 201 events (1997 - 2007) through a direct comparison between data and synthetics based upon a centroid moment tensor inversion [Liu et al. (2004)]. Initial evaluations were done using a 1D reference model [Dziewonski and Anderson (1981)] at periods greater than 80 seconds and a more stringent evaluation was done for 3D model [Kustowski et al. (2008)] at periods of 25 seconds and longer. Final source reinterpretations within the 3D model define a source database and the initial starting point for the adjoint tomography. Transitioning from a 1D to 3D wave speed model shows dramatic improvements when comparisons are done at shorter periods (25 s) and even at longer periods (80 s). Synthetics from the 1D model were created through mode summations while those from the 3D simulations were created using the spectral element method.

Finally, updates of the wave speed model were accomplished using adjoint tomography. Initial inversion iterations have guided the measurements, model smoothing and filtering to produce the accurate and relevant improvements to the initial model. Initial attempts to update the wave speed model were hampered by the strong anisotropy in the mantle causing an unavoidable mismatch between Rayleigh and Love waves when using an isotropic mantle parameterization. Relaxing constraints on the mantle wave speeds to allow for transverse isotropy with a vertical symmetry axis allowed the fitting of both surface waves and thus continued improvement of the wave speed model and inclusion of even shorter periods.

Event kernels are computed “quickly” at the n-th iteration and invert for a new *(n+1)*-th wave speed model of the Middle East. As demonstrated with previous adjoint tomography experiments [Tape et al. (2009)], each iteration improves the model progressively, and relies on successive iterations to reduce variance and improve the fitting of data to synthetics. Exploiting the source database with multiple adjoint inversions at shorter and shorter periods will refine the wave speed structures of the Middle East. Inversion results demonstrate that the iterative nature of the adjoint tomography improves the travel time variations between synthetics and data primarily, with less of an improvement to the waveform amplitudes. Iterative improvements also significantly increase anomaly strength while sharpening the anomaly edges to create stronger and more pronounced tectonic structures. The results presented here, while accurate at intermediate periods, require the addition of attenuation tomography and a transverse isotropy without a vertical symmetry axis to further reduce the minimum period towards travel time tomography models.

OBJECTIVES

Improved 3D wave speeds of the greater Middle East, from the Turkish Plateau to the eastern edge of Tibet (Figure 1), enhances our ability to discriminate between natural and man-made events, locate these events, identify source depths, and determine magnitudes using waveform based methodologies. Current wave speed models of the Middle East are improved through an adjoint tomography method [Tromp et al., 2005] by a comparison of seismic phase and amplitude data. An initial step towards the adjoint tomography model requires the development of a database of relocated and well-characterized set of sources and waveforms. Events were re-inverted in 1D and 3D wave speed models and agree fairly well with currently available solutions. Use of a 3D model improves the waveform fit between data and synthetics and reduces the overall error of the CMT solution. The adjoint tomography method [Tromp et al., 2005] uses full seismic waveforms as a measure of misfit of the current model iteration. Differences between data and synthetics are used to create adjoint sources and generate sensitivity kernels required to update the wave speed model. The final round of iterations amplify and sharpen wave speed anomalies in the Middle East while increasing the predictive capabilities at periods of 15 seconds and longer. The adjoint tomography model was built on the foundation of the seismic waveform database and finite-frequency wave propagation, and will be distributed to the community.

RESEARCH ACCOMPLISHED

Event Characterization

Approximately 200 events in the Middle East were re-characterized using the CMT inversion methodology of Liu et al. [2004] and the 1D PREM model [Dziewonski and Anderson, 1981] at periods of 25 / 60 seconds and longer and within a 3D wave speed model (S2.9EA) [Kustowski et al., 2008]. A map of all available stations and events are shown in Figure 1. Initially, the procedure of processing large amounts of data, comparing these to synthetics, and reevaluating the source parameters and locations needed to be assessed and streamlined. This procedure, accomplished through the use of a 1D wave speed model and long period modeling, needed to be straightforward and nimble enough to avoid problematic areas, as the initial 3D event re-evaluation requires more demanding computational efforts. Problematic events and stations were subsequently screened out within this procedure before building the final waveform data set was implemented in the adjoint inversion. Problematic stations and waveforms with dropouts and poorly characterized amplitude responses can negatively influence a CMT inversion, and these stations were removed before any 3D CMT inversions or adjoint inversions were performed.

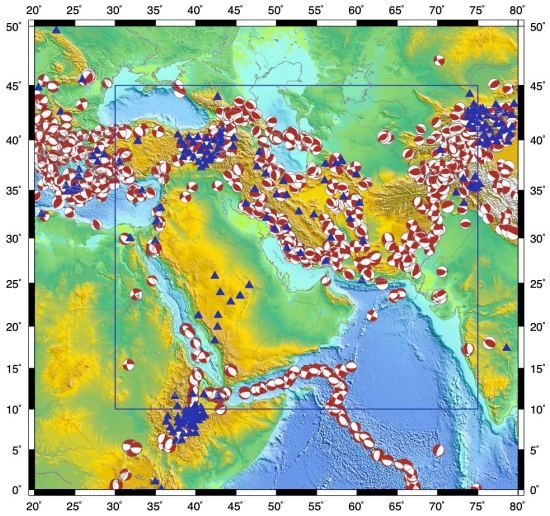

Figure 1. Map of the available sources and stations in the Middle East for the adjoint tomography inversion.

Solutions using the 3D wave speed model at periods of 25 seconds and longer are shown in Figure 2. Faulting parameters agree well with those from the Global CMT Project. Solutions match reasonably well when using either 1D or 3D wave speed models, but use of the 3D wave speed model allows prediction of complexity in body wave arrivals and more pronounced surface wave arrivals and dispersion. The CMT inversion procedure automatically identifies windows to use as constraints [Maggi et al, 2009], and use of the 3D wave speed model results in more time windows and subsequently a larger portion of the full waveform included in the CMT inversion. Windows must exceed stringent minimums over all metrics for inclusion in the inversion.

Performance of the CMT inversion is highlighted in Figure 3. The assess the performance of the CMT inversion, the p-axis was used as it reduces a complex system with up to 9, Mij, parameters down to 2, strike and dip. This assumes the events are primarily double couple with minimal isotropic or compensated linear vector dipole components. Results from a bootstrap procedure on a single event are shown on in the left panel of Figure 3. Focal spheres for 1D and 3D wave speed models are shown for reference. Similar to what is demonstrated in Figure 3, for each event and each wave speed model, a bootstrap was performed to determine the standard error of the strike and dip of the p-axis. Standard errors for the entire data set for the strike and dip are shown in Figure 3, center and right panels. Over the full data set, the standard error of the solution decreases when using the 3D model over the 1D model at 25 – 125 seconds period. The reduction in solution error is also apparent at periods of 60 – 125 seconds.

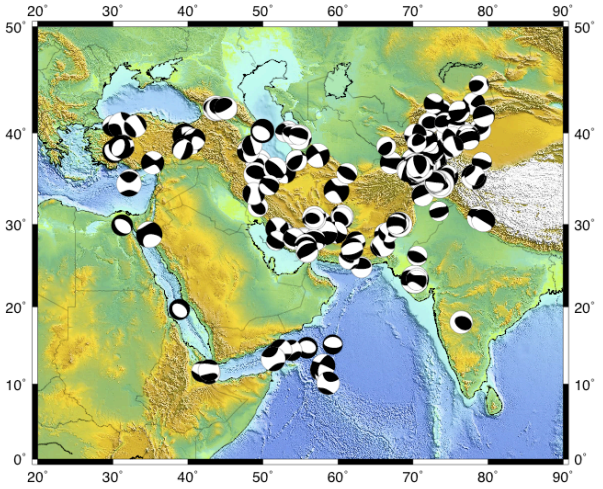

Figure 2. Source database derived from the 3D wave speed model at 25 second and longer

Adjoint Inversions and Model Updates

Using the differences between the synthetic and observed seismograms, an event kernel is constructed for each source using the adjoint method [Tromp et al. 2005]. The sum of all these event kernels guides model updates for the current iteration. Automatic measurements are made between the data and synthetics using the Flexwin tool [Maggi et al., 2009], creating data windows and associated metrics that are then used in the creation of adjoint sources. Windows, and their adjoint sources, are not constrained to any specific seismic phase or time window and only use well matched data-synthetic pairs. Adjoint sources along with the reconstructed, full synthetic wavefield are propagated in reverse time through the current iteration wave speed model to identify locations in the model requiring improvement. Interactions between the adjoint sources and the time-reversed wavefield, integrated over time, generate kernels specific to each measurement, e.g. a simple difference between the data and synthetics. Such kernels can be created using individual, isolated measurements or for each event with a large number of back-propagated adjoint sources. Event kernels are then summed volumetrically to produce Frechet derivates that are used to update the wave speed model.

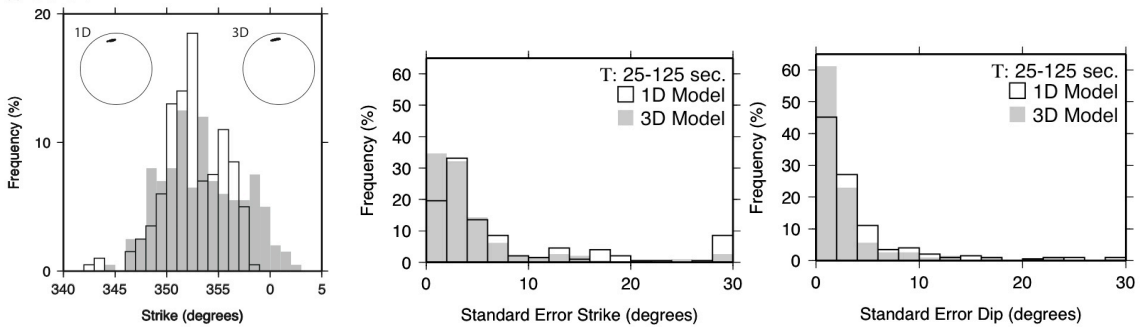

Figure 3. Performance of the CMT inversion when using the 1D (white) and 3D (gray) wave speed models. Left panel shows a histogram of p-axis strikes from a bootstrap procedure for a single event. Focal spheres for 1D and 3D with all p-axes from the bootstrap shown for reference. Center (right) panel shows the standard error of the strike (dip) of the p-axis for the entire data set. Use of the 3D wave speed model reduces the standard error over the entire data set.

In a first attempt, our updates to the wave speed model used a steepest descent method and an isotropic mantle wave speed along with tight controls on the magnitude of the update. The maximum change in the model update was limited to 3% based on comparisons between data and synthetics from a set of test events not used in the inversion. As a result of the parameterization the shear wave speed model oscillated between each iteration step. The inversion was attempting to fit the Rayleigh and Love waves simultaneously. Due to the long period nature of these surface waves they are primarily sensitive to mantle wave speeds. An isotropic parameterization of the mantle is unable to satisfy the known transversely isotropic mantle and as such the subsequent model iterations oscillated between two local minima. From these initial tests, addition of an anisotropy parameterization, as transverse isotropy, of the mantle fit the Rayleigh and Love wave simultaneously and allowed further incorporation of shorter period arrivals. With this new parameterization, finer scale structures began to appear and large-scale oscillations were eliminated with each iteration.

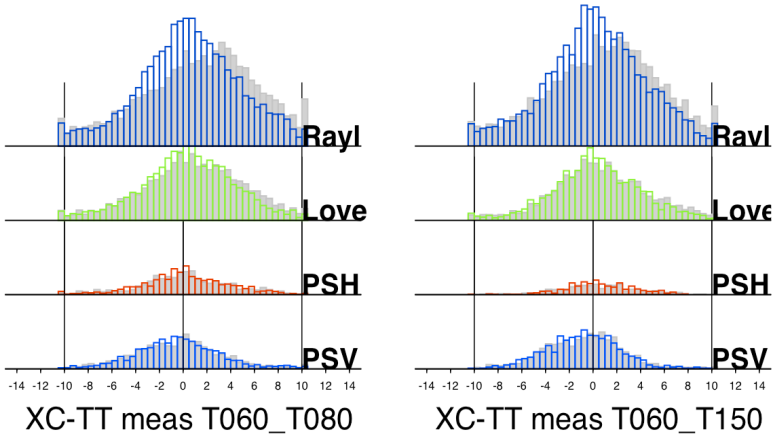

Figure 4. Comparison of travel time measurements between the initial model, gray, and the current iteration model, colors, made using cross correlation. Measurements are separated by wave type including Rayleigh (Rayl) and Love waves, and body waves on the vertical-radial components (PSV) and transverse component (PSH). Two different bandpasses are shown.

Figure 4 shows the travel time performance of the current iteration model against the starting wave speed model. In general, travel time variations are reduced at long periods for the Rayleigh and Love waves. The total misfit between the data and synthetics as measured by metrics from Flexwin, time shift, amplitude ratio, and cross-correlation value, all show progressive improvement to the synthetics relative to the data for each iteration. Amplitude ratios show less of an improvement when compared to travel time. The small improvement in amplitude is due to a combination of the lack of even shorter periods in the inversion and incorrect attenuation structure. Currently a 1D attenuation structure is used throughout the model domain, but addition and improvement to a 3D attenuation model are realizable by using the amplitude misfit for all arrivals and the adjoint, amplitude kernels defined in Tromp et al. [2005].

Progression of the wave speed model for a sample set of iterations is shown in Figure 5 as absolute shear wave speeds, Vsv and Vsh. The oscillations previously identified are not apparent in this set of iterations due to the incorporation of transverse isotropy, Vsv and Vsh. As the number of iterations increase, improvements are applied to the model and shorter period date are included in the inversion. With these improvement and shorter period data higher resolution structures begin to appear in the wave speed model. Two examples of new higher resolution structures are in the Red Sea in Vsv and in the South Caspian Sea in Vsh. It is interesting to note the wave speed model prefers reductions in wave speed in Vsv and increases in wave speed as Vsh; a feature that would not be possible without transverse isotropy in the mantle and the fitting of both Love and Rayleigh waves.

A set of comparisons, waveforms and cross-sections, between the current iteration and the starting model (S2.9EA) are contained in Figure 6. Waveform fits from a path from southern Zagros to station KBK demonstrates that updates to the model are improving the fit between data and synthetics. This event is not included in the adjoint tomography, but is used to provide a consistency check on the models improvement and progression. After about a third of the total iterations a lower wave speed Vsv lithosphere is required in the middle of this path, to the southwest of Tibet's western syntaxis. This lower wave speed region appears in the cross sections, but also apparent in the synthetics. The surface wave in the starting model arrives earlier than the data, but arrives "on-time" using the current iteration model.

The initial model in central Asia at 100 km depth shows faster wave speeds caused primarily by thick, cold lithosphere. Further to the south, into the Zagros Mountains where a large amount of continental deformation and crustal thickening is occurring, the wave speeds are substantially slower. This Asian north-to-south, fast-to-slow wave speed pattern in the initial model is mirrored in the current iteration, Figures 5 and 6. Similar behavior was identified in other finite-frequency tomography experiments [Montelli et al., 2004]. Wave speed perturbations in the initial model are amplified when using sensitivity kernels based on a finite-frequency approach rather than an approximation, either classical ray theory or surface wave sensitivities kernels. Large continuous and anomalous

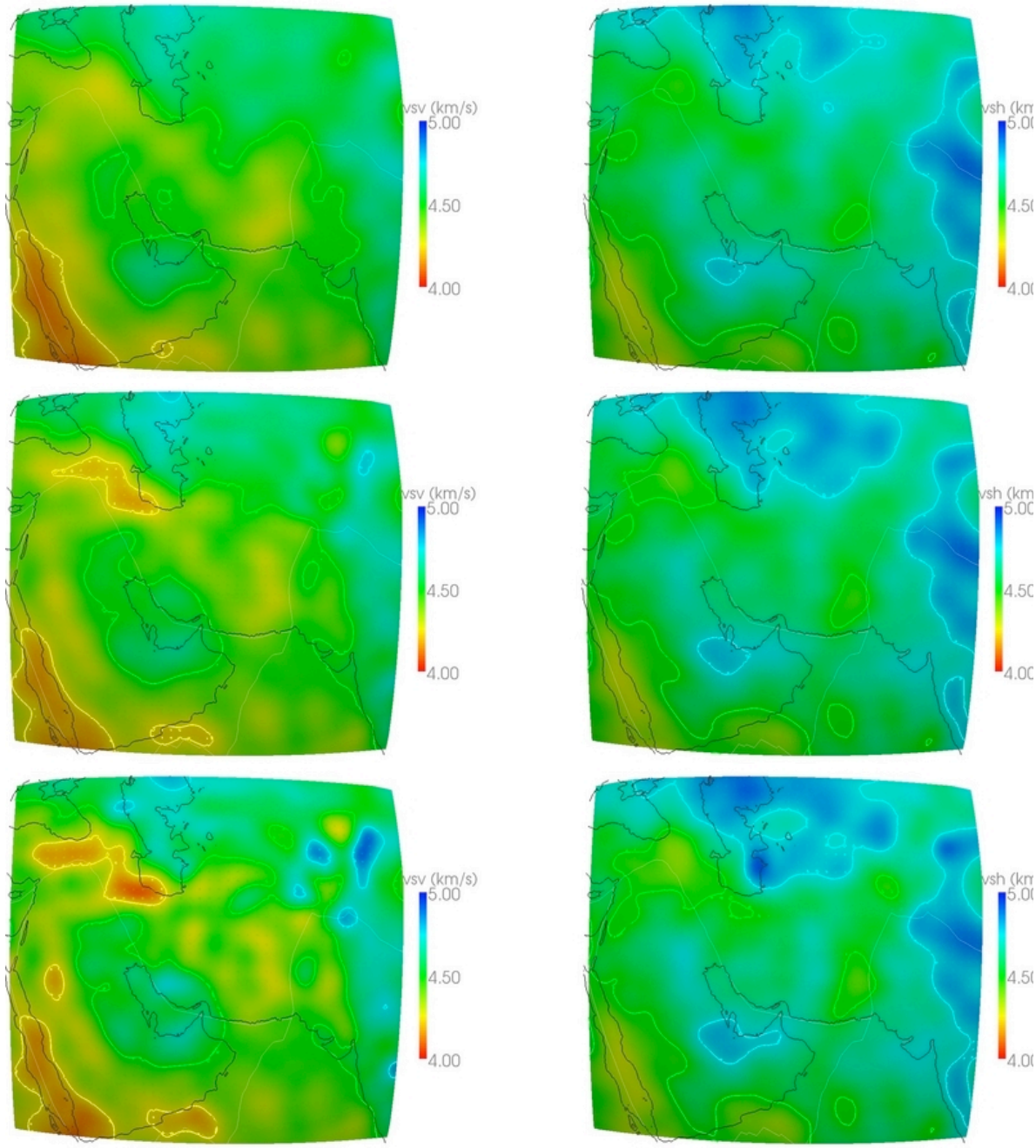

Figure 5. Comparison of the Middle East wave speed model at different iterations. The left column is Vsv and the right column is Vsh. The top row is the initial wave speed model, the second row is the 3rd iteration and the bottom row is the 6th iteration. Model depth is 100 km.

regions in the initial model, Figure 5, will become stronger and begin to separate into individual anomalies as the more iterations are completed.

Updates to the model also include density and compressional components. The initial 3D compressional wave speed model was scaled in the initial model from the 3D shear wave speed by a constant factor. Shear wave speeds in S2.9EA were derived from a large number of Love, Rayleigh, and shear body. A comparison between the compressional adjoint results and the initial model can be difficult as the ratio between shear and compressional wave speeds can vary due to composition. All adjoint iterations for compressional wave speeds show a much slower upper mantle beneath much of the Middle East than indicated by S2.9EA. Updates to the model at long wavelengths for these initial iterations are predominately controlled by Rayleigh waves (shear and compressional surface wave) as the initial S2.9EA model fit the Love waves (shear only surface waves) better, Figures 4 and 5.

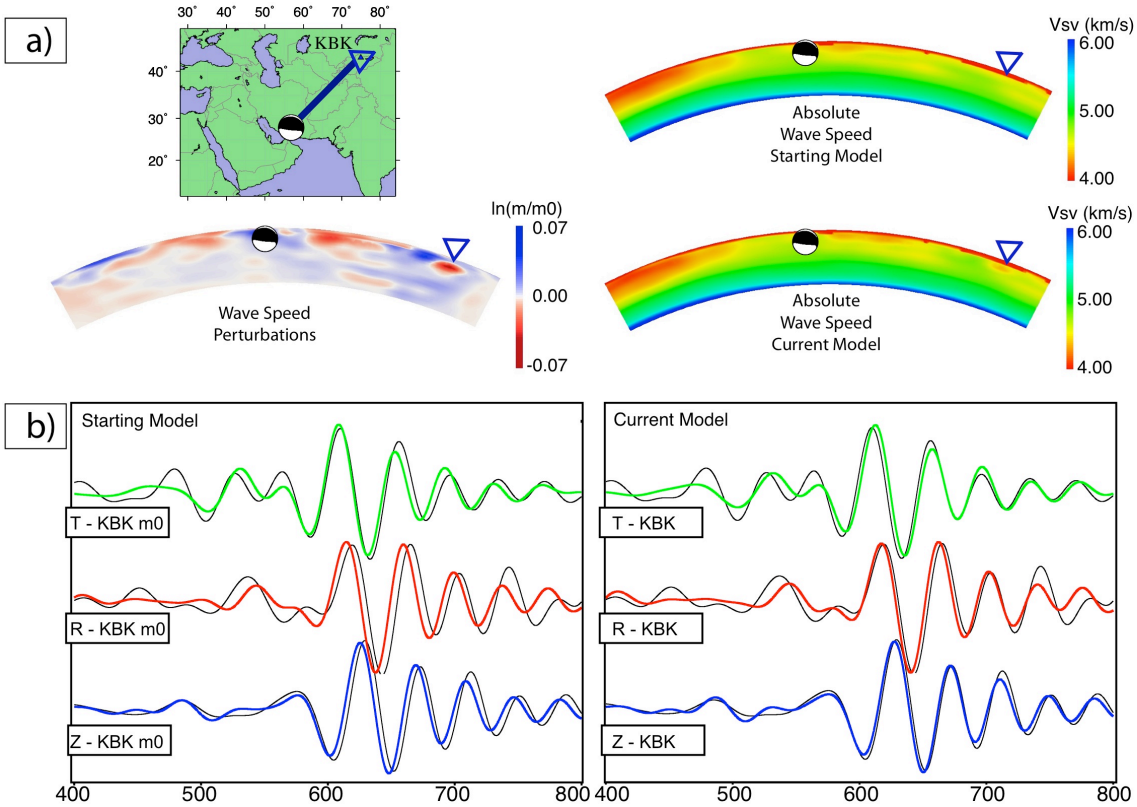

Figure 6. Demonstration of the current iteration model through a single station – event pair. The station, KBK, and event, southern Zagros, are not included in the adjoint tomography. Panel a) includes a location map and a cross-section with relative wave speeds between the initial model, m0, and the current model, m. Panel a) also includes the same cross-section but as absolute wave speed, Vsv. Panel b) shows the improved fit of the waveforms between the starting, left, and current models, right. Data is black and synthetics are plotted in color.

CONCLUSIONS AND RECOMMENDATIONS

Adjoint iterations to update the wave speed model of the Middle East have shown dramatic improvements to the model based on data / synthetic comparisons and expected behavior when introducing a finite-frequency tomographic approach. Before iterations began, a seismic waveform database with ~200 reinterpreted sources in the Middle East was compiled to avoid the mapping of source errors into wave speed structure. All sources in the database agree with previously published solutions and between the methodologies used: CAP [Zhao and Helmberger, 1994], teleseismic [Kikuchi and Kanamori, 1982] and a CMT inversion [Liu et al., 2004]. Initial

comparisons between data and synthetics computed from the initial 3D model S2.9EA [Kustowski et al., 2008] at 25 seconds and longer show reasonable agreement and a general improvement over the 1D PREM model [Dziewonski and Anderson, 1981]. To further improve the fit between data and synthetics, the adjoint inversion methodology was implemented to iteratively update the 3D wave speed model [Tromp et al., 2005]. Following an initial set of iterations, the wave speed model was parameterized to incorporate transverse isotropy in the mantle to accommodate the simultaneous fitting of Rayleigh and Love waves. This parameterization helped to stabilize the inversion and allowed further inclusion of shorter periods into the adjoint tomography. As the model progresses through a series of iterations, regions of wave speed anomalies have increased in strength from the initial to the current iteration as physics of wave propagation were incorporated into the inversion; see, e.g., the Red Sea and the southern Caspian Sea, Figure 5. Compressional wave speed estimates also improved from increased use of Rayleigh waves. Our recommendations for a robustly constrained 3D wave speed model in the Middle East include using quality controlled seismic waveform data from well-constrained sources and use of a physics based tomographic technique to improve upon existing 3D models. Further recommendations to improve the wave speed model include adding:

- anisotropic effects where necessary, e.g. the mantle, and
- attenuation to improve fits to amplitudes and
- shorter period signals to further improve the waveform predictive capabilities of the wave speed model of the Middle East.

REFERENCES

Dziewonski, A., and D. Anderson (1981), Preliminary reference Earth model, *Phys. Earth. Planet. Int.*, *25*, 297–356.

Kikuchi, M., and H. Kanamori (1982), Inversion of complex body waves, *Bull. Seism. Soc. Am.*, *72*(2), 491–506.

Komatitsch, D., and J. Tromp (1999), Introduction to the spectral-element method for 3-D seismic wave propagation, *Geophys. J. Int.*, *139*, 806–822.

Kustowski, B., G. Ekstrom, and A. Dziewonski (2008), The shear-wave velocity structure in the upper mantle beneath eurasia, *Geophys. J. Int.*, *174*, 978–992, 10.1111/j.1365-246X.2008.03865.x.

Liu, Q., J. Polet, D. Komatitsch, and J. Tromp (2004), Spectral-Element Moment Tensor Inversions for Earthquakes in Southern California, *Bull. Seism. Soc. Am.*, *94*(5), 1748–1761, 10.1785/012004038.

Maggi, A., C. Tape, M. Chen, D. Chao, and J. Tromp (2009), An Automated time-window selection algorithm for seismic tomography, *Geophys. J. Int.*, *178*(1), 257–281, 10.1111/j.1365-246X.2009.04099.x.

Montelli, R., G. Nolet, F. Dahlen, G. Masters, E. Engdahl, and S. Hung (2004), Finite-Frequency Tomography Reveals a Variety of Plumes in the Mantle, *Science*, *303*(5656), 338–343.

Tape, C., Q. Liu, A. Maggi, and J. Tromp (2009), Adjoint tomography of the Southern California crust, *Science*, *325*, 988–992.

Tromp, J., C. Tape, and Q. Liu (2005), Seismic tomography, adjoint methods, time reversal and banana-doughnut kernels, *Geophys. J. Int. 160*(1), 195–216.

Zhao, L., and D. Helmberger (1994), Source estimation from broadband regional seismograms, *Bull. Seism. Soc. Am.*, *84*(1), 91–104.

Prepared by LLNL under Contract DE-AC52-07NA27344.